Modelling of Stress-Strain Relationships of Mortar with Blast Furnace Slag Fine Aggregates under Static Loading in Air and Water

Hokkaido University	Student member	○Muhammad Aboubakar Farooq
Hokkaido University	Regular Member	Yasuhiko Sato
Okayama University	Regular Member	Toshiki Ayano
Oriental Shiraishi Corporation	Regular Member	Kyoji Niitani

1. INTRODUCTION

Due to environmental considerations and strict regulations, numerous research is being carried out to use industrial wastes in concrete industry because it will not only reduce the need to landfill these wastes, but it will also minimize the environmental loads, energy consumption and depletion of natural resources. Blast furnace slag (BFS) is among one of such industrial wastes; generated during the production of iron and steel. This slag is a by-product obtained by quenching molten iron slag from blast furnace in water or steam to produce glassy and granular product that is then dried and ground into fine powder or sand particulates. In Japan, volume of granulated blast furnace slag produced is over 20 million tons per annum and 90% of it is used as a material for cement and concrete production **[1]**.

Concrete containing granulated blast furnace slag (GBFS) is well known for improving its properties due to pozzolanic activity of GBFS resulting in dense matrix, high strength at long-term age and better durability properties like water tightness, chemical resistance and chloride ion permeation **[1]**. Valcuende et al. (2015) found that early age compressive strength of concrete with GBFS sand is almost similar to the concrete with river sand, but the compressive strength improves at longer age with increased replacement of fine aggregates by slag **[2]**. On contrary, it is pointed out that high quantity of non-ground GBFS as fine aggregates results in high porosity and less compressive strength of concrete **[3,4]**. However, in the recent years, it has been found that the durability related properties of mortar and concrete can be greatly improved by the use of ground GBFS as percentage of binder and with the incorporation of BFS as total amount of fine aggregates. It is reported that the mortar and concrete containing BFS fine aggregates show significant resistance against various severe environmental actions like frost damage, corrosion **[5,6]**. In addition, significant improvement in resistance was observed when mortar and concrete with BFS were exposed to sulfuric acid compared to ordinary one **[7]**. However, the mechanical characteristics of BFS mortar and concrete are not clarified yet. To apply such material in reinforced concrete (RC) structures subjected to mechanical loading, it is essential to have relevant understanding of the various conditions that ensures durable concrete performance.

This paper demonstrates the experimental investigation of mortar with BFS sand in compression compared with ordinary mortar containing crushed sand (CS) in air and water. Thereafter, the stress-strain relationships for both types of mortar are formulated under monotonic loading in air and water. The experimental results are compared with those of calculated using proposed model, which show good agreement between the two.

2. EXPERIMENTAL DETAILS

2.1 Materials and Mix Proportions

Two series of mortar specimens were casted, blast furnace slag (BFS) mortar and crushed sand (CS) mortar. Ordinary Portland cement (OPC) was used as binder in both types of mortar. The density of OPC is 3.15 g/cm^3, while the Blaine fineness is 3300 cm^2/g. In the preparation of BFS mortar specimens, BFS sand is used as full amount of fine aggregates while crushed river sand is used for CS mortar specimens. Fine aggregates with particle size of 0.3 to 5 mm are used in this study. Table 1 presents the mix proportion of BFS mortar and CS mortar. The cement to sand ratio is kept as 1:2. The polycarboxylate type of high range water reducing admixture is used as an additional admixture.

2.2 Specimens and Test Method

The cylindrical specimens were casted with diameter of 50 mm and height of 100 mm in steel molds for each type of mortar. After demoulding, the specimens were cured in normal water for seven days. The top casted surface of the cylindrical specimens was ground to make it smooth and parallel to the hinge surface placed between loading platen and specimen. For strain measurement, two vertical and two horizontal strain gauges of 30 mm gauge length were attached to the surface of the specimens. The vertical and horizontal strain gauges were attached parallel and perpendicular to the axial loading direction respectively using epoxy resin.

The uniaxial static compression tests were carried out on three cylindrical specimens of each BFS mortar and CS mortar in air at the age of 1-year in accordance with JIS A1108:2006 **[8]**. The static compression test was performed in

Table 1: Mix proportions of blast furnace slag mortar and crushed sand mortar

Mortar Type	W/C (%)	Unit Content (kg/m^3)				HRWRA (kg/m^3)	AFA (kg/m^3)
		W	C	BFS	CS		
BFS	35	268.5	767	1533	0	3.84	2.30
CS		271.6	776	0	1552		

W: Water content, C: Ordinary Portland cement, HRWRA: High range water reducing admixture, AFA: Antifoaming agent.

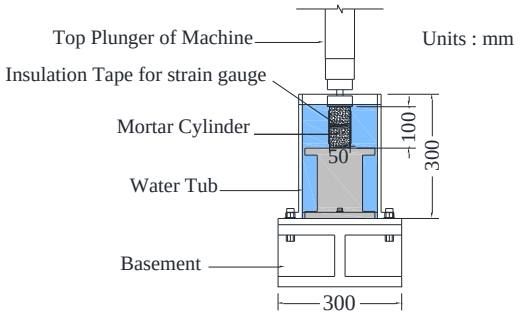

Figure 1: Loading arrangement

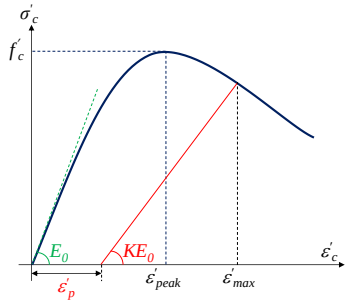

Figure 2: Stress-strain relationship

air using displacement control at a rate of 0.01 mm/sec. Thereafter, the static compression test was performed in water on three specimens of each mortar. The strain measurement was made by the attached strain gauges to the specimens. Prior to testing in water, the strain gauges were protected with water proof adhesive tape to prevent the moisture effect on strain measurement and specimens were submerged in water for 48-hours before testing for uniform saturation inside the specimen. The loading arrangement is shown in Fig. 1.

3. RESULTS AND DISCUSSION

The average compressive strength (f'_c), Young's modulus (E), Poisson's ratio (v) and strain at ultimate strength (ε'_{peak}) of each mortar in air and in water are summarized in Table 2. BFS mortar showed more compressive strength than CS mortar both in air as well as water. The compressive strength of both types of mortar was decreased in water because the adsorbed water layers due to saturation reduce the surface energy of hydration product significantly due to surface tension of water. This leads to remarkable reduction of fracture energy and strength of mortar. Especially CS mortar has pronounced tendency of reducing compressive strength in water because CS mortar specimens have more voids and water absorption capacity compared to BFS mortar, therefore the surface energy of CS mortar is reduced by large amount resulting in more reduction in compressive strength. It is reported that higher the voids and liquid content of cement based material lead to large reduction in surface energy **[9]**.

BFS mortar in water shows greater Young's modulus than CS mortar in air despite of lower compressive strength of BFS mortar in water. Moreover, BFS mortar showed more Young's modulus compared to CS mortar both in air and water.

4. STRESS-STRAIN RELATIONSHIPS

4.1 Formulation of Model

The stress-strain relationships for BFS mortar and CS mortar proposed in this study are based on the elasto-plastic and fracture (EPF) model for concrete developed by Maekawa and Okamura (1983) **[10]**. In EPF model, the stress-strain relationship is given as shown in Fig. 2 and Eq. (1).

$$\sigma'_c = KE_0(\varepsilon'_{max} - \varepsilon'_p) \tag{1}$$

Where σ'_c is compressive stress, ε'_{max} is maximum strain and ε'_p is plastic strain. K is the fracture parameter and E_0 is the Young's modulus of concrete. Fracture parameter (K) and plastic strain (ε'_p) are the function of maximum strain (ε'_{max}) and strain corresponding to ultimate strength (ε'_{peak}).

The mechanical properties of concrete such as strength, stiffness and deformation characteristics are affected differently compared to that of mortar under the application of load, because of absence of coarse aggregates in mortar. Therefore, the equations for fracture parameter (K) and plastic strain (ε'_p) developed for concrete in EPF model **[10]** are not applicable for mortar. For that reason, the static unloading and reloading tests on cylindrical specimens of BFS mortar and CS mortar were carried out to measure the stiffness and plastic strain at unloading both in air and water. The specimens were prepared using the same procedure as explained earlier. The mortar specimens were loaded to some value and then unloaded to zero value. This procedure was repeated for four loading cycles and then the specimen was loaded to the failure.

The stiffness and plastic strain of each loading cycle for each mortar is measured. The experimental data is fitted to get the relation for fracture parameter (K) for both types of mortar in air as well as in water. The relationship for the fracture parameter (K) for BFS mortar and CS mortar in air as well as in water is formulated as given as in Eq. (2):

$$K = exp\left\{-0.43\left(\frac{\varepsilon'_{max}}{\varepsilon'_{peak}}\right)^{exp\left(0.95\frac{\varepsilon'_{max}}{\varepsilon'_{peak}}\right)}\left(1-exp\left(-0.74\frac{\varepsilon'_{max}}{\varepsilon'_{peak}}\right)\right)\right\} \tag{2}$$

The fracture parameter (K) calculated by Eq. (2) for both mortars in air and water is shown in Fig. 3 along with the change in fracture parameter for concrete calculated by the EPF Model. It can be seen that the fracture parameter of concrete decreases sharply compared to that of mortar due to coarse aggregates. The values of fracture parameter (K) for mortar calculated by the Eq. (2) are compared with those of obtained from the experimental data. The average experimental values of fracture parameter are close to the calculated values ($\overline{K}_{exp.}/\overline{K}_{cal.}$=1.01) with a coefficient of variation (COV) of 2.8% showing the good agreement

Table 2: Mechanical properties of blast furnace slag mortar and crushed sand mortar

Test Condition	Mortar Type	f'_c (MPa)	E (GPa)	v	$\varepsilon'_{peak}(\mu)$
Air	BFS	109	40.6	0.28	3492
	CS	104	34.9	0.26	4270
Water	BFS	101	39.6	0.30	3117
	CS	87	33.8	0.25	3490

f'_c: Compressive strength, E: Young's modulus, v: Poisson's ratio, ε'_{peak}: strain value at ultimate compressive strength

between the two as presented in Fig. 4.

Plastic deformation is defined as the damage which is not recoverable even after the removal of load. The equations for the plastic strain of BFS mortar and CS mortar in air as well as in water are developed by using the experimental data of static unloading and reloading test as shown in Eq. (3).

$$\varepsilon_p^{'} = \varepsilon_{peak}^{'}.exp\left(-a+bln\left(\frac{\varepsilon_{max}^{'}}{\varepsilon_{peak}^{'}}\right)\right) \quad = 0 \text{ at } \varepsilon_{max}^{'} = 0 \qquad (3)$$

Where a and b are the constant and the respective values are shown in Table 3 for both types of mortar in air and water. The input for the plastic strain equation are the value of strain corresponding to the ultimate strength of respective mortar as given in Table 2 and maximum strain along with value of constant a and b. The plastic strain for each mortar in air as well as in water calculated by the proposed equation given in Eq. (3) is normalized by ($\varepsilon_{peak}^{'}$) of each mortar and is shown in Fig. 5 along with the normalized plastic strain calculated for normal concrete calculated by EPF Model.

It can be seen from the figure that more plastic strain is developed in concrete compared to mortar because of more plasticity caused by damage of bond between coarse aggregates and mortar in concrete. The CS mortar showed more plastic strain development than BFS mortar in air and water. The reason for more plastic strain development in CS mortar is that the bond between fine aggregates and matrix may be weak as compared to BFS mortar. Moreover, the size of fine aggregates in CS mortar and voids are more resulting

Table 3: Value of constant a and b for BFS and CS Mortar

Test Condition	Mortar Type	Constant a	Constant b
Air	BFS	2.96	1.66
	CS	2.07	1.99
Water	BFS	3.54	1.62
	CS	2.39	2.15

in more plastic strain due to collapse of voids and bond compared to that of BFS mortar. However, less plastic strain is produced for both types of mortar compared to air.

The comparison between calculated plastic strain values of each mortar by Eq. (3) is made with the experimental values as shown in Fig. 6. There is satisfactory agreement between the calculated plastic strain values and experimental ones ($\varepsilon_{p,exp.}/\varepsilon_{p,cal.}$=0.998) with a COV of 22.7%. The high value of COV is due to disparity between the calculated and experimental plastic strain values of CS mortar in air.

Poisson's ratio (v), which is defined as the negative ratio between the transverse strain to the axial strain. To calculate the stress-lateral strain curve, the equations for Poisson's ratio for BFS mortar and CS mortar are formulated by using the experimental values. The Poisson's ratio of BFS mortar and CS mortar be calculated for certain maximum normalized axial strain by Eq. (4) and Eq. (5) respectively, in air and water. The Poisson's ratio for both BFS mortar and CS mortar remained constant before axial strain ratio of 0.8 and after that it started to increase.

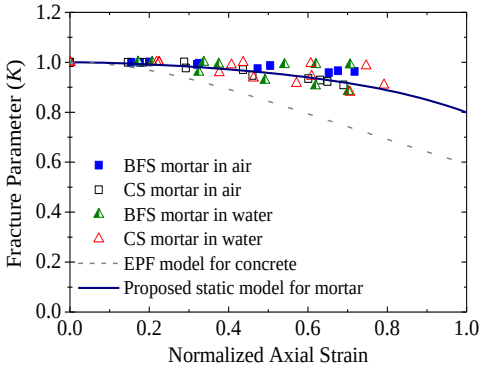

Figure 3: Fracture parameter for each mortar in air and water along with normal concrete

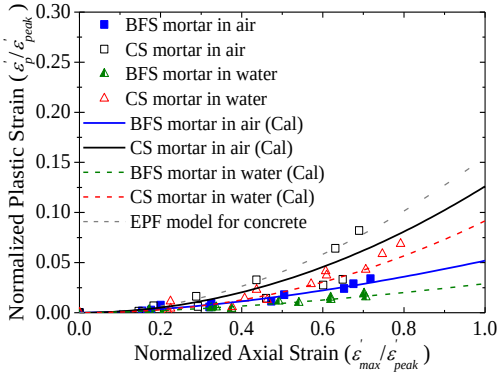

Figure 5: Plastic Strain development for BFS mortar and CS mortar in air and water along with normal concrete

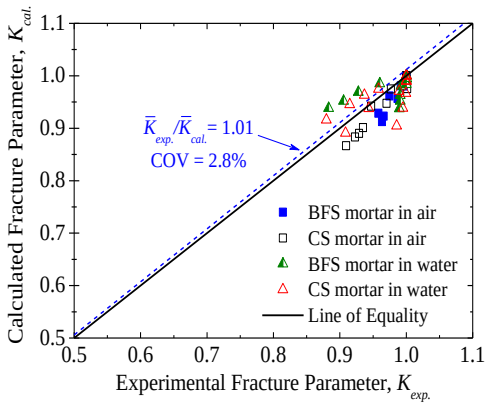

Figure 4: Comparison between calculated fracture parameter and experimental fracture parameter of mortar

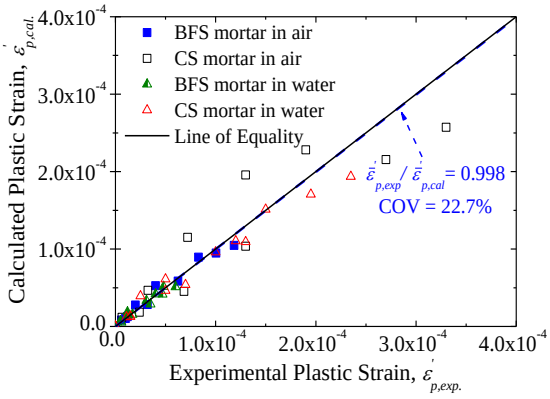

Figure 6: Comparison between calculated plastic strain and experimental plastic strain values of mortar

$$\nu = 0.28;\ \text{for}\ \left(\varepsilon'_{max}/\varepsilon'_{peak}\right) \le 0.8$$
$$\nu = 0.28 + 1.25\left(\frac{\varepsilon'_{max}}{\varepsilon'_{peak}} - 0.8\right)^2;\ \text{for}\ \left(\varepsilon'_{max}/\varepsilon'_{peak}\right) > 0.8 \quad (4)$$

$$\nu = 0.25;\ \text{for}\ \left(\varepsilon'_{max}/\varepsilon'_{peak}\right) \le 0.8$$
$$\nu = 0.25 + 1.75\left(\frac{\varepsilon'_{max}}{\varepsilon'_{peak}} - 0.8\right)^2;\ \text{for}\ \left(\varepsilon'_{max}/\varepsilon'_{peak}\right) > 0.8 \quad (5)$$

5. CORRELATION BETWEEN PROPOSED MODEL AND EXPERIMENT

The stress-strain relationships for both BFS mortar and CS mortar are calculated in air and water using the proposed model as given in Eq. (1). The input parameters are the maximum axial strain, strain at ultimate compressive strength and Young's modulus of each mortar presented in Table 2. The fracture parameter and plastic strain for mortar are calculated by using Eq. (2) and Eq. (3) respectively. The stress vs. transverse strain curves are obtained by using the Poisson's ratio equations for BFS mortar and CS mortar as shown in Eq. (4) and Eq. (5). The calculated stress-strain relationships for BFS mortar and CS mortar in air and water are drawn in Fig. 7 along with average curves obtained from the experiments. It can be seen that the calculated stress-strain curves are close to the experimental ones.

The ultimate compressive strength of BFS mortar and CS mortar obtained by the proposed model are compared with those of measured during experiment in air and water as shown in Fig. 8. The good agreement between the average of experimental ultimate compressive strength and calculated by the proposed model ($f'_{c,cal.}/\ f'_{c,exp.}$=0.98) is obtained with COV of 2.14%. It proves that the proposed model is valid and can be used for analysis of structural elements with mortar.

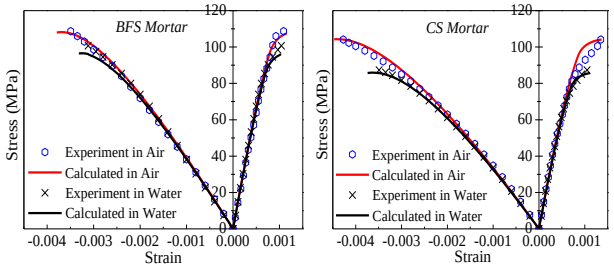

(a) BFS mortar　　(b) CS mortar

Figure 7: Comparison between experimental and calculated stress-strain curves in air and water

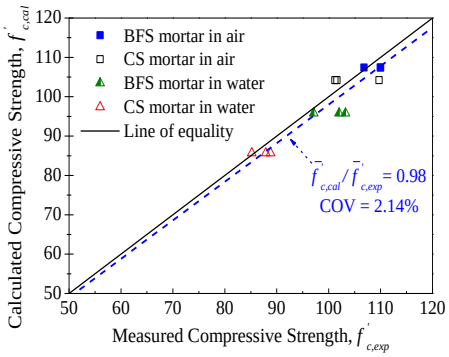

Figure 8: Comparison between experimental and calculated compressive strengths

6. CONCLUSIONS

Following conclusions can be drawn from this study:

- BFS mortar exhibits more compressive strength compared to CS mortar both in air and water. When static test was performed in water, the static compressive strength of BFS mortar and CS mortar was decreased by 7% and 16% respectively compared to static compressive strength in air because saturation inside the mortar causes reduction of surface energy and leads to earlier failure.
- The stress-strain model for each mortar under static loading is formulated based on elasto-plastic and fracture model. The rate of plastic strain development and stiffness reduction of mortar are slower than those of the concrete. Therefore, relationships for plastic strain and fracture parameter are formulated.
- The proposed model in this study provides good agreement with the experimental results.

ACKNOWLEDGEMENT

This work was supported by Council for Science, Technology and Innovation, "Cross-ministerial Strategic Innovation Promotion Program (SIP), Infrastructure Maintenance, Renovation, and Management". (funding agency: NEDO)

REFERENCES

[1] Statistical annual report of iron and steel slag. Nippon Slag Association, Japan, 2011, pp. 2-3.
[2] Valcuende M., Benito F., Parra C. and Miñano I. Shrinkage of self-compacting concrete made with blast furnace slag as fine aggregate. Journal of Construction and Building Materials, 2015; 76, pp. 1-9.
[3] Yüksel I., Özkan Ö. and Bilir T. Use of granulated blast-furnace slag in concrete as fine aggregate. ACI Material Journal, 2006; 103(3), pp. 203-8.
[4] Yüksel I., Genç A. Properties of concrete containing non-ground ash and slag as fine aggregate. ACI Material Journal, 2007;104(4), pp. 397-403.
[5] Fujii T. and Ayano T. Freezing and thawing resistance of concrete with blast furnace slag. International Conference on Non-Traditional Cement and Concrete, 2014; Vol. 0X.
[6] Jariyathitipong P., Hosotani K., Fuiji T. and Ayano T. Strength and durability of concrete with blast furnace slag. Third Intl. Conference on Sustainable Construction Materials and Technologies, Kyoto, Japan, 2013.
[7] Jariyathitipong P., Hosotani K., Fuiji T. and Ayano T. Sulfuric acid resistance of concrete with blast furnace slag fine aggregates. Journal of Civil Engineering and Architecture, ISSN 1934-7359, 2014; 8, pp. 1403-13.
[8] JIS A1108:2006, Standard Test Method for Compressive Strength of Concrete, 2006.
[9] Matsushita H. and Onoue K. Influence of Surface Energy on Compressive Strength of Concrete under Static and Dynamic Loading. Journal of Advanced Concrete Technology, 2006; Vol. 4, No. 3, pp. 409-421.
[10] Maekawa K. and Okamura H. The deformational behavior and constitutive equation of concrete using elasto-plastic and fracture model. Journal of the Faculty of Engineering, The University of Tokyo, 1983; XXXVII (2), pp. 253-328.